

CrossMark  
click for updatesCite this: *Phys. Chem. Chem. Phys.*,  
2016, **18**, 2143

# Interlocking order parameter fluctuations in structural transitions between adsorbed polymer phases

Paulo H. L. Martins<sup>a</sup> and Michael Bachmann<sup>abc</sup>

By means of contact-density chain-growth simulations of a simple coarse-grained lattice model for a polymer grafted at a solid homogeneous substrate, we investigate the complementary behavior of the numbers of surface–monomer and monomer–monomer contacts under various solvent and thermal conditions. This pair of contact numbers represents an appropriate set of order parameters that enables the distinct discrimination of significantly different compact phases of polymer adsorption. Depending on the transition scenario, these order parameters can interlock in perfect cooperation. The analysis helps understand the transitions from compact filmlike adsorbed polymer conformations into layered morphologies and dissolved adsorbed structures, respectively, in more detail.

Received 24th August 2015,  
Accepted 7th December 2015

DOI: 10.1039/c5cp05038c

[www.rsc.org/pccp](http://www.rsc.org/pccp)

## 1. Introduction

Polymers are complex systems that often tend to form structures without apparent symmetries. This makes it difficult to analyze the cooperative behavior of the individual monomers that leads to structure formation. Furthermore, systematic experimental studies of individual polymers of finite size are sophisticated and results often do not possess sufficient resolution to identify characteristic features of compact structures. This leaves computer simulations the only tool for thorough investigations, although for scans of parts of environmental and material parameter spaces these studies are limited to rather simple models.

Lattice polymer models are among the most common to study generic features of structure formation processes. Structural transitions of individual self-interacting lattice polymers, which in the simplest case are self-avoiding walks<sup>1,2</sup> with local non-bonded interactions,<sup>3–10</sup> and lattice proteins<sup>10–23</sup> have been studied extensively in the past. Whereas scaling properties of polymer transitions between disordered and loosely ordered phases, such as the  $\Theta$  collapse transition, could be investigated by means of simulations of large systems rather easily (see, for example, the discussion and references in ref. 9 and 24), the

analysis of compact solid phases remains a difficult problem.<sup>7–9,25</sup> The simulation of appropriate system sizes is hardly possible. For certain types of polymers, such as proteins, the study of finite-size properties is more relevant than the large-scale behavior,<sup>10</sup> but for homopolymers the study of larger systems is beneficial and allows for scaling analyses.

Studies of the adsorption behavior of polymers and proteins near attractive substrates have been popular for quite some time. As for the understanding of the folding behavior of single polymers, lattice models of hybrid organic–inorganic systems have also been employed largely to understand the statistical mechanics of polymer adsorption and constrained structure formation near such a boundary.<sup>26–39</sup>

In this paper, we investigate properties of order parameters that are suitable to distinguish compact filmlike polymer structures adsorbed on a homogeneous substrate (AC1) from adsorbed expanded conformations (AE) that represent a gaslike macrostate on the substrate. We also investigate the transition that separates the two-dimensional compact single-layer AC1 phase and the compact and globular adsorbed phases with multiple layers (AC2&AG). These structural phases extend into the third dimension perpendicular to the substrate, which is why it is a topological dewetting transition.

The structure of the paper is as follows. In Section II, we introduce the hybrid lattice polymer–substrate adsorption model and describe the chain-growth approach to the systematic generation of interacting self-avoiding walks near an attractive substrate. The statistical mechanics of microphases is discussed in Section III and used to construct the canonical structural phase diagrams in Section IV. The paper is concluded by the summary in Section V.

<sup>a</sup> Instituto de Física, Universidade Federal de Mato Grosso, 78060-900 Cuiabá, MT, Brazil. E-mail: pmartins@fisica.ufmt.br

<sup>b</sup> Soft Matter Systems Research Group, Center for Simulation Physics, The University of Georgia, Athens, GA 30602, USA. E-mail: bachmann@smsyslab.org; Web: <http://www.smsyslab.org>

<sup>c</sup> Departamento de Física, Universidade Federal de Minas Gerais, 31270-901 Belo Horizonte, MG, Brazil

## II. Lattice model of polymer adsorption and chain growth

For our study of the thermodynamic adsorption properties of a polymer with  $N$  monomers tethered to a homogeneous substrate, we employ a minimalistic interacting self-avoiding walk model (ISAW) on a simple-cubic lattice. Energetically, a monomer favors nearest-neighbor contacts with other nonbonded monomers and with the attractive substrate. Therefore, by introducing the total numbers of monomer–surface contacts  $n_s$  and monomer–monomer contacts  $n_m$ , the energy of a single polymer conformation can simply be expressed by

$$E_s(n_s, n_m) = -\varepsilon_0(n_s + sn_m), \quad (1)$$

where  $\varepsilon_0$  is the overall (irrelevant) energy scale that will be set to unity in the following. The parameter  $s$  represents the ratio of energy scales associated with intra-monomer contact formation and substrate binding, respectively. Physically, it can be interpreted as a reciprocal solvent quality parameter, because a larger positive value supports the formation of compact polymer structures (poor solvent), whereas smaller values favor stronger binding to the substrate and, therefore, the effective dissolution of conformations (good solvent). Fig. 1 shows as an example a conformation of a polymer with 503 monomers as found in the simulations. It has  $n_s = 5$  monomer–surface and  $n_m = 154$  monomer–monomer contacts.

In this study, we consider  $s$  as a system or material parameter, and the temperature  $T$  as an environmental control parameter for the canonical statistical ensemble of the system coupled to a heatbath. Both parameters together govern the energetic and entropic system behavior and thus enable the construction of a hyperphase diagram that accounts for the transition between classes of macrostates of the system, which in the following we will simply call “phases”.<sup>10</sup>

Simulations of different system sizes with up to  $N = 503$  monomers were performed by employing the contact-density chain-growth algorithm,<sup>10</sup> which samples the  $(n_s, n_m)$  contact number space directly and completely. The result is the contact density  $g(n_s, n_m)$ , which is simply given by the number of

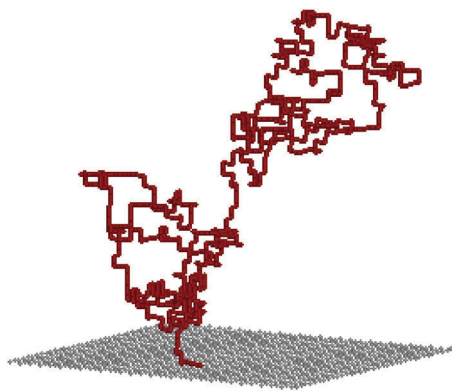


Fig. 1 Example of a conformation with 503 monomers as found in the chain-growth simulations of the lattice polymer model of adsorption used in this study. One end of the chain is grafted at the substrate.

polymer conformations with  $n_s$  surface and  $n_m$  monomer–monomer contacts. As we will discuss later, these contact numbers suit perfectly as order parameters that enable the discrimination of most adsorbed and desorbed structural phases of the polymer. The energy-free representation of the “density of states” is also extremely convenient as it allows for the reweighting of energetic quantities to any desired system and environmental condition (in  $T$ - $s$  space) after the simulation has been performed.

The contact-density chain-growth method is a generalization of multicanonical<sup>10,20,21</sup> and flat-histogram<sup>40</sup> versions of the pruned-enriched Rosenbluth method (PERM)<sup>6</sup> and its nPERM extensions.<sup>18,19</sup> PERM is a significant improvement of the original Rosenbluth method.<sup>1</sup> Generally, in chain-growth methods, the polymer chain is typically grown from the first bead. Since the bond length is fixed, only nearest-neighbor sites are available for placing the next bead. An unoccupied nearest-neighbor site is chosen to extend the chain by adding another monomer. If the number of unoccupied nearest-neighbor sites of the current chain end point is  $m_l$ ,  $l = 1, \dots, N - 1$ , then one of those lattice sites is chosen with probability  $m_l^{-1}$  as the new end point of the chain. The procedure is continued until the chain has reached its final length ( $N$  monomers) or if it got stuck in a “dead end”, where no continuation is possible. In order to sample the configuration space to get appropriate statistics for further analysis, the Rosenbluth chain-growth method is repeated many times. The method obviously creates a bias which needs to be corrected by assigning each chain, created in this way, an own weight,  $W_R = \prod_{l=1}^{N-1} m_l$ . If the algorithm is repeated a large number of times  $M$ , the mean of the Rosenbluth weight  $\overline{W}_R \approx \sum_{i=1}^M W_R^{(i)} / M$  is a good estimator for the absolute total number of possible polymer conformations.

In PERM,<sup>6</sup> at each step the Rosenbluth weight is multiplied by the Boltzmann factor containing the energetic change caused by this step. Furthermore, enriching the sample by creating copies of chains with large weights and pruning chains with less promising weights increases the sampling efficiency. The result is an absolute estimate of the canonical partition function. In the multicanonical variants,<sup>10,20,21,40</sup> pruning and enriching is based on weight functions that result in a flat energy histogram by artificially enhancing the population of entropically suppressed states during the simulation. These methods provide absolute estimates for the density of states.

Fig. 2 shows the contact density for a lattice polymer with 503 monomers as obtained in our simulations. The contact density covers more than 300 orders of magnitude. Note that the chain-growth method is capable of creating absolute estimates, in contrast to importance-sampling Monte Carlo methods. This is particularly beneficial if an estimate for the ground-state degeneracy is needed such as in studies of designing sequences of lattice proteins.<sup>20,21</sup>

## III. Statistical mechanics of the micro-contact ensemble

The standard canonical partition function that can be written as a sum over all microstates with energy  $E$  and their degeneracy

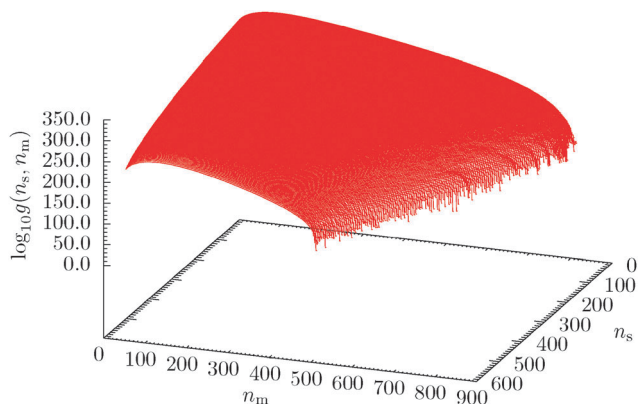


Fig. 2 Contact density distribution  $g(n_s, n_m)$ , *i.e.*, the number of states with  $n_s$  contacts with the substrate and  $n_m$  monomer–monomer contacts of a polymer with 503 monomers.

(number of states)  $\hat{g}(E)$  can also be expressed by means of the contact numbers

$$Z_{T,s}^{\text{can}} = \sum_{E_s} \hat{g}(E_s) e^{-E_s/k_B T} = \sum_{n_s, n_m} Z_{T,s}(n_s, n_m). \quad (2)$$

Here, we have introduced the restricted partition function in contact number (or order parameter) space:

$$Z_{T,s}(n_s, n_m) = g(n_s, n_m) e^{-E_s(n_s, n_m)/k_B T}. \quad (3)$$

With this, we can introduce the free energy, parametrized by  $s$  and  $T$ , as a function of the contact numbers:

$$F_{T,s}(n_s, n_m) = -k_B T \ln Z_{T,s}(n_s, n_m). \quad (4)$$

By introducing the conformational contact entropy  $S(n_s, n_m) = k_B \ln g(n_s, n_m)$ , we can also write the free energy in the common form

$$F_{T,s}(n_s, n_m) = E_s(n_s, n_m) - TS(n_s, n_m). \quad (5)$$

Note that the free-energy landscapes for all values of the temperature  $T$  and solvent quality  $s$  can be obtained easily, in principle, by reweighting from the contact density after a single simulation run. If one accepts that  $n_s$  and  $n_m$  are appropriate order parameters, the global minimum of the free-energy landscape for each parameter pair  $(T, s)$ ,

$$F_{T,s}^{\text{min}} = F_{T,s}(n_s^{\text{min}}, n_m^{\text{min}}), \quad (6)$$

represents the dominant macrostate  $(n_s^{\text{min}}, n_m^{\text{min}})_{T,s}$  in contact number space. If upon variation of  $T$  and  $s$ , the macrostate does not change within a certain environment  $\varepsilon(T, s)$  of the parameter space, *i.e.*,  $(n_s^{\text{min}}, n_m^{\text{min}})_{\varepsilon(T,s)} = (n_s^{\text{min}}, n_m^{\text{min}})_{T,s}$ , we call this section of the parameter space a “stable microphase”. Structural phases can then be defined as ensembles of macrostates (or microphases) sharing characteristic (structural) features.

It is worth mentioning that the contact definition can be extended to continuum models as well by introducing effective energy ranges or threshold distances.<sup>41</sup>

## A. Microphase free-energy landscapes

Fig. 3 shows the microphase diagram for a polymer with 503 monomers in the section of the parameter space relevant for our study. Each cell corresponds to a microphase representing the same macrostate  $(n_s^{\text{min}}, n_m^{\text{min}})$ . Although it is not easily possible to combine microphases in order to identify structural phases, three regions can be distinguished, in which the sizes of the cells significantly differ. As we will see later, the interfaces between these regions fall together with transition lines of structural transitions. In the lower right part of the figure, we find very small cells, *i.e.*, each of the many connected microphases is unstable. This is an indication that the entire structural phase possesses high entropy and is disordered. In the upper right part, microphases cover larger regions in parameter space, meaning that overall they are more stable and ordered. The wedge-shaped part to the left is highly ordered and since the  $s$  value is comparatively small (*i.e.*, surface contacts are favored), this structural phase is dominated by strong adsorption effects.

A complementary approach to the discussion of phase diagrams based on free-energy landscapes is the identification and mapping of all free-energy minima in  $(n_s, n_m)$  space for any desired  $(T, s)$  parameter pair. Therefore, by scanning sufficiently large regions in  $(T, s)$  space and determining the corresponding free-energy minimum locations (*i.e.*, the macrostates)  $(n_s^{\text{min}}, n_m^{\text{min}})$ , it is also possible to identify structural phases and even to determine the character of the transitions in-between (continuous or discontinuous). The map of all free-energy minima  $(n_s^{\text{min}}, n_m^{\text{min}})$  identified for the 503mer in the temperature region  $T \in [0, 10]$  and for solvent parameter values in the interval  $s \in [0, 10]$  is shown in Fig. 4. Shaded regions correspond to structural phases, *i.e.*, the conformations associated with the free-energy minima possess characteristic similarities.

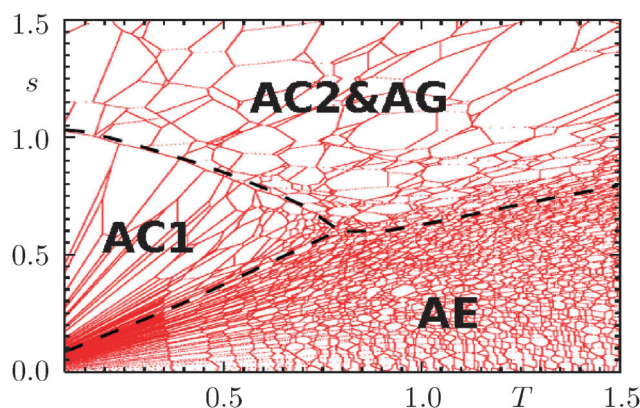


Fig. 3 Structural microphase diagram for the 503mer adsorbed at a substrate from the free-energy perspective. Each dot in this graph represents a change of the location of the free energy minimum  $F_{T,s}^{\text{min}} = F_{T,s}(n_s^{\text{min}}, n_m^{\text{min}})$  in the space of the contact numbers  $(n_s, n_m)$ , by varying temperature  $T$  and solvent quality  $s$ . The dashed lines correspond to the ridges of the specific-heat landscape (see Fig. 6) and correspond well to the boundaries of the cell structure of the microphase diagram. Deviations are caused by finite-size effects.

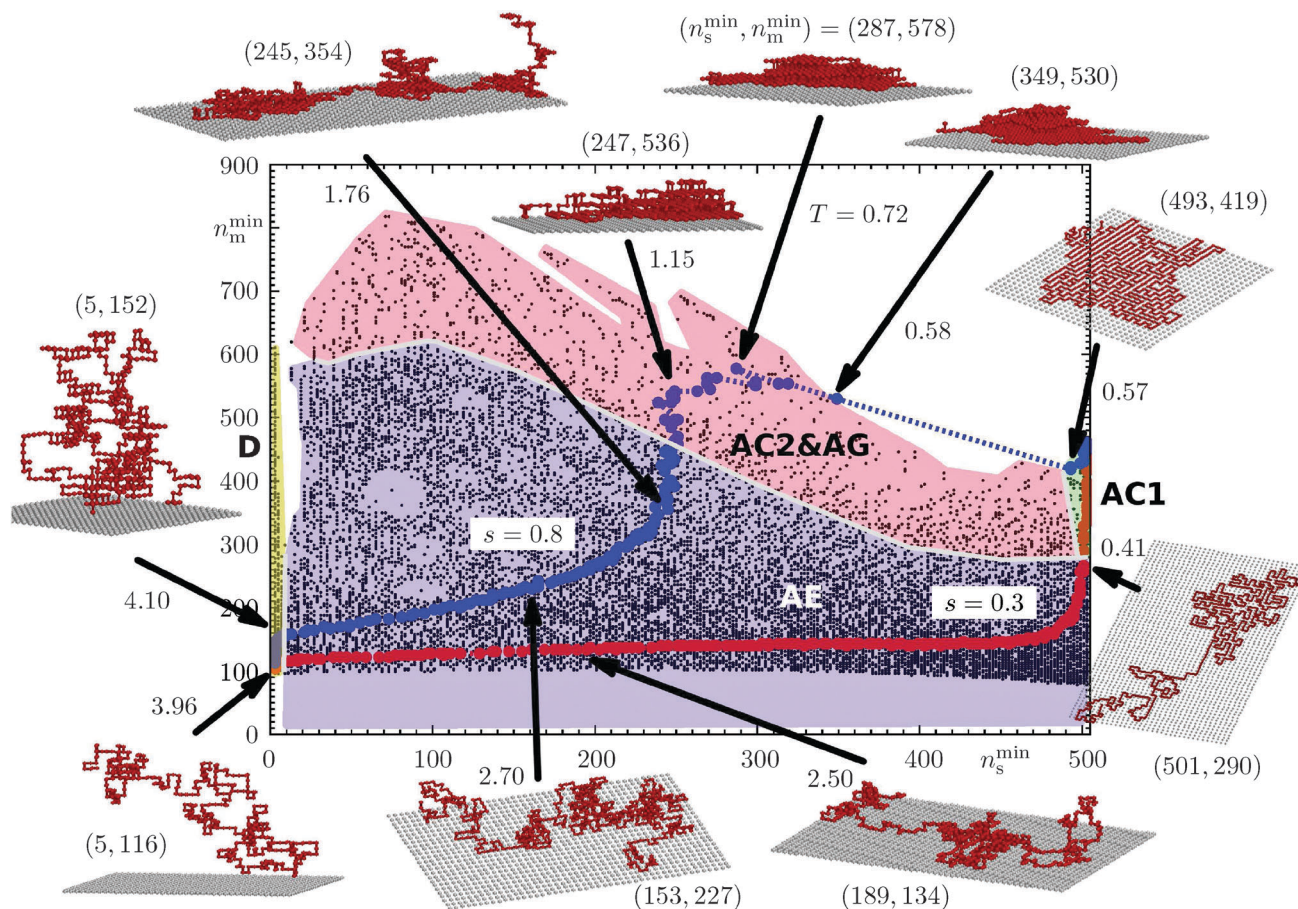


Fig. 4 Map of all global free-energy minima located at contact number values  $n_{s,m}^{\min}$  in the intervals of temperatures  $T \in [0,10]$  and solvent parameters  $s \in [0,10]$  for a lattice polymer with 503 monomers grafted at a solid substrate. The trajectories shown for  $s = 0.3$  and  $0.8$  connect the corresponding free-energy minima at all temperatures in the given interval. This provides insight into the differences of the conformational changes in contact-number space upon adiabatically changing the temperature under good and poor solvent conditions. Also shown are representative conformations at selected temperatures along those minimum free-energy paths. The numbers close to the arrows correspond to the selected values of the temperature  $T$ . In parentheses next to each sample conformation, the contact numbers  $(n_s^{\min}, n_m^{\min})$  that are associated with the free-energy minimum are given.

## B. Solvent effects

It is instructive to follow two thermal trajectories through this landscape by increasing the temperature successively at a constant value of  $s$ . From Fig. 3, we find  $s = 0.3$  and  $0.8$  interesting choices, because the cuts in  $T$ -direction at these values cross different transition lines. The temperature dependence of the free-energy minimum locations  $n_{s,m}^{\min}$  is depicted in Fig. 5. At zero temperature, both trajectories start in the filmlike regime, which we label AC1 (adsorbed-compact, single layer). While all monomers are in contact with the substrate (*i.e.*,  $n_s^{\min} = 503$ ), the number of monomer-monomer contacts of the lowest-energy conformations found in the simulations is  $n_m^{\min} = 461$  for both  $s$  values.

**1. Good solvent.** By adiabatically increasing the temperature, the number of surface contacts of the free-energy minimum configuration remains widely stable, but under the good solvent conditions present at  $s = 0.3$ , the compactness of the filmlike structure decreases. At about  $T = 0.41$ , this change is most rapid: the polymer undergoes a transition from the compact AC1 phase into more disordered, but still mostly two-dimensional microstates

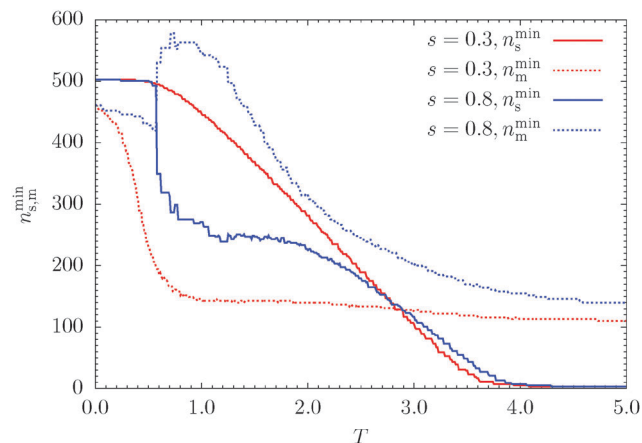


Fig. 5 The contact numbers  $n_{s,m}^{\min}$  at the global free-energy minima as a function of temperature for  $s = 0.3, 0.8$ .

in the adsorbed-expanded (AE) phase of polymer conformations. The number of monomer-monomer contacts drops below  $n_m^{\min} = 150$  before  $T = 1.0$  is reached. Conformations that resemble

random coils extend more and more in the direction perpendicular to the substrate. The effect of the good solvent is two-fold: polymer structures dissolve and previously adsorbed monomers are released off the substrate.

As Fig. 5 shows,  $n_s^{\min}$  drops steadily over a large temperature interval until, near  $T = 4.0$ , almost all monomers have lifted off and enjoy the additionally available transitional entropy. The polymer has reached the desorbed phase D in its random-coil regime (desorbed expanded), where it is quasi-free in the available space that grafting permits. If the polymer was not grafted, but confined in a sufficiently large volume, it would completely desorb and the large translational entropy would cause a (first-order-like) phase separation between the adsorbed and desorbed phases,<sup>30,31,42,43</sup> although the transition is strictly continuous in the thermodynamic limit.<sup>44</sup>

**2. Poor solvent.** Under poor solvent conditions, as present for  $s = 0.8$ , the structural behavior of the polymer upon adiabatic heating is significantly different. As can be seen in Fig. 5, the macrostates characterized by  $n_{s,m}^{\min}$  are very stable in the compact phase of basically two-dimensional filmlike structures AC1 at low temperatures below  $T = 0.57$ . At this point a topological transition occurs. While in good solvent ( $s = 0.3$ ) the polymer passes the transition  $AC1 \Leftrightarrow AE$  continuously, the crossover from AC1 into the neighboring phase is a phase-separation process. Structurally, the polymer forms additional layers which increase the number of monomer–monomer contacts at the expense of surface contacts. Structures remain compact, but are three-dimensional.

For  $s = 0.8$ , the monomer arrangement in this phase is not particularly ordered, which is why we denote the phase as adsorbed globular (AG). Note that at even higher  $s$  values the polymer transitions into much more ordered double-layer states (AC2: adsorbed-compact with two or more layers).<sup>30,31</sup> For  $s = 0.8$ , characteristic conformations at the coexistence point are shown in Fig. 4. Upon increasing the temperature to  $T = 0.72$ , the number of monomer–monomer contacts increases further slightly (from  $n_m^{\min} = 530$  to 578), while the number of surface contacts continues to diminish. The structural response to the thermal environment remains almost the same until  $T \approx 1.15$  is reached. Then, it changes radically. Between  $T = 1.15$  and  $T = 1.76$ , the number of monomer–monomer contacts drops rapidly from  $n_m^{\min} = 536$  to 354 at almost constant number of surface contacts ( $n_s^{\min} = 247$  vs. 245). The compact polymer structure disintegrates while going through the transition from AC2&AG to AE. From here on, the behavior at higher temperatures is similar to that in the good-solvent scenario, *i.e.*, solvent effects are less relevant, although structures remain more compact when the system experiences the desorption transition, entering phase D, at about  $T = 4.10$ .

## IV. Canonical analysis of structural phases

In this section, we investigate the hyperphase diagram of polymer adsorption, parametrized by temperature  $T$  and solvent quality  $s$ ,

from the perspectives of fluctuations of energy and interlocking contact numbers.

### A. Canonical structural phase diagrams

The contact density  $g(n_s, n_m)$  enables immediate access to all thermodynamic quantities that depend on  $n_{s,m}$ . Because of the model definition, eqn (1), this includes all energetic quantities. Since we have already identified the contact numbers as useful order parameters for the characterization of the structural transitions between the phases AC1, AC2&AG, and AE, the investigation of the thermal fluctuations of these quantities is beneficial as well. By means of the restricted partition function (3), the canonical statistical average of any quantity  $O$  that is a function of  $n_s$  and  $n_m$  is given by

$$\langle O(n_s, n_m) \rangle(T, s) = \frac{1}{Z_{T,s}^{\text{can}}} \sum_{n_s, n_m} O(n_s, n_m) Z_{T,s}(n_s, n_m), \quad (7)$$

with the canonical partition function  $Z_{T,s}^{\text{can}}$  from eqn (2). The conformational energy  $E_s$  associated with the model (1) and the contact numbers that we consider as order parameters in this study are the most basic quantities of interest.

For the study of enhanced thermal activity in response to adiabatic changes of environmental parameters such as temperature or external fields, it has always been useful to introduce response quantities. These are commonly defined as the derivatives of order parameters with respect to the external field that causes the perturbation. The most prominent response quantity is the heat capacity of the system, which quantifies the amount of energy necessary to readjust the temperature of the system to the environmental heat-bath temperature. An extremal fluctuation is typically associated with a qualitative change in the system, which we consider here as a phase transition in the general sense that includes finite systems. The corresponding order parameter is the energy. It is a general and therefore unspecific order parameter, because it does not normally offer much insight into the physical nature of the transition. In the context discussed in this paper, extremal fluctuations of the energy ( $E_s$ ) upon a change of the temperature  $T$  represent a significant qualitative alteration of the geometric structure of the polymer.

We introduce any thermal response quantity in the form

$$\begin{aligned} \Gamma_O(T, s) &= \frac{d\langle O \rangle(T, s)}{dT} \\ &\equiv \frac{1}{k_B T^2} [\langle O E_s \rangle(T, s) - \langle O \rangle(T, s) \langle E_s \rangle(T, s)]. \end{aligned} \quad (8)$$

Therefore,  $\Gamma_{E_s}(T, s) = C_V(T, s)$  defines the heat-capacity profile in  $(T, s)$  space. The specific-heat profile for the 503mer in this space is shown in Fig. 6. Cuts at  $s = 0.3$  and  $0.8$  are plotted in Fig. 7. The canonical phase diagram covers the same region as the microphase diagram depicted in Fig. 3, where dashed lines represent the ridge lines of the specific-heat profile. Slight deviations in the location of these estimates for transition lines and the boundaries of the cell structure in Fig. 3, particularly apparent for the transition between AC2&AG and AE, are due to the finite size of the system. Finite-size effects broaden

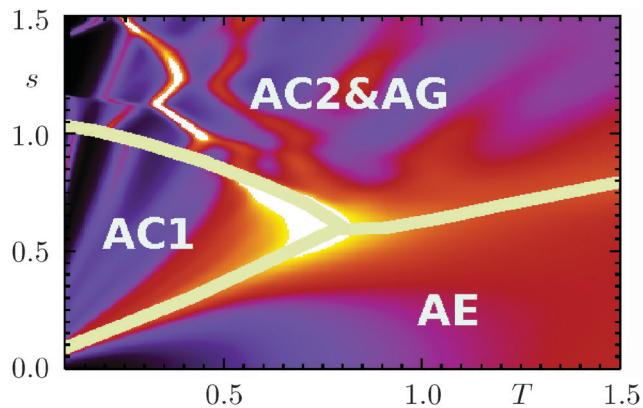


Fig. 6 Color-coded specific-heat profile  $C_V(T,s)$  representing the part of the structural hyperphase diagram of the 503mer that features the transitions between filmlike, two-dimensional adsorbed conformations (AC1), adsorbed expanded structures (AE), and adsorbed multi-layer compact and globular polymer morphologies (AC2&AG).

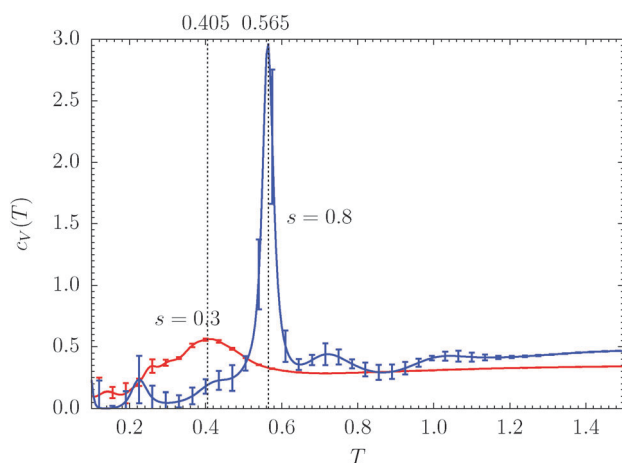


Fig. 7 Cuts through the specific-heat profile in Fig. 6 at solvent parameter values  $s = 0.3$  and  $0.8$  for the 503mer.

distributions of canonical quantities such as the energy distribution. In the canonical statistical analysis, averages calculated from these distributions and the extremal fluctuations about this mean at the transition point are used to locate the transition point. The solid lines in the specific-heat landscape in Fig. 6 represent the regions of extremal energy fluctuations. However, the thus determined transition parameters do not necessarily match the microcanonical estimates, which are more unique as microcanonical thermodynamics does not allow for fluctuations. Therefore, microcanonical analysis methods enable a more universal definition of transition points in finite systems, which is why these techniques have become more popular recently in the context of studies of polymer systems.

For the fluctuations of the contact numbers  $n_{s,m}$  that we have identified as useful specific order parameters in the discussion in the previous sections, we can derive similar expressions. If we denote the second-order cumulant of two quantities  $x$  and  $y$  by  $\langle xy \rangle_c = \langle xy \rangle - \langle x \rangle \langle y \rangle$ , where  $x$  and  $y$  can be

either  $n_s$  or  $n_m$ , the contact-number correlation matrix can be written as

$$M = \begin{pmatrix} \langle n_s^2 \rangle_c & \langle n_s n_m \rangle_c \\ \langle n_s n_m \rangle_c & \langle n_m^2 \rangle_c \end{pmatrix}. \quad (9)$$

Therefore, trivially, one can introduce unit state vectors

$$\mathbf{e}_{n_s} = \begin{pmatrix} 1 \\ 0 \end{pmatrix}, \quad \mathbf{e}_{n_m} = \begin{pmatrix} 0 \\ 1 \end{pmatrix} \quad (10)$$

that project the system state into the spaces of monomer-surface and monomer-monomer contacts. Effectively, each contact represents a “quasi-particle” and the variances of the total number of contacts in these spaces can be written as  $\langle n_{s,m}^2 \rangle = \mathbf{e}_{n_{s,m}}^T M \mathbf{e}_{n_{s,m}}$ . More important in our context is the introduction of contact-number fluctuations. If we introduce the energy scale vector

$$\boldsymbol{\varepsilon} = \varepsilon_0 \begin{pmatrix} 1 \\ s \end{pmatrix} = \varepsilon_0 (\mathbf{e}_{n_s} + s \mathbf{e}_{n_m}) \quad (11)$$

for the monomer-surface (first component) and monomer-monomer contacts (second component), respectively, the fluctuations can be expressed by

$$\Gamma_{n_{s,m}} = -\frac{1}{k_B T^2} \boldsymbol{\varepsilon}^T M \mathbf{e}_{n_{s,m}}. \quad (12)$$

The fluctuation profiles of the contact numbers are shown in Fig. 8 as density plots. Large fluctuations are represented by bright colors and help indicate regions of rapid changes of the order parameters. Dashed lines are inserted to mark the phase boundaries as identified from the specific-heat profile shown in Fig. 6. Expectation values of the contact numbers and horizontal cuts through the landscapes of the contact-number fluctuations at  $s = 0.3$  and  $0.8$  are depicted in Fig. 9 and 10, respectively.

Using eqn (9) and (11), the heat capacity simply reads

$$\Gamma_{E_s} = \frac{1}{k_B T^2} \boldsymbol{\varepsilon}^T M \boldsymbol{\varepsilon}. \quad (13)$$

Because of the minimal coupling of the energetic contributions in the model (1) and the corresponding separation of the energy scales in contact-number space (11), we can immediately write down an important relation between the energetic and the order-parameter fluctuations in  $(T,s)$  space:

$$\Gamma_{E_s}(T,s) = -\varepsilon_0 [\Gamma_{n_s}(T,s) + s \Gamma_{n_m}(T,s)]. \quad (14)$$

This means that signals in the heat capacity like peaks or “shoulders”, indicating structural transitions in the finite system, can be directly related to order-parameter fluctuations.

## B. Interlocking

In particular, if the heat capacity is extremal as a function of  $T$ ,  $d\Gamma_{E_s}/dT = 0$  in finite systems, as it is at the structural transition point, then eqn (14) leads to the correlation relation

$$\frac{d\Gamma_{n_s}(T,s)}{dT} = -s \frac{d\Gamma_{n_m}(T,s)}{dT}, \quad (15)$$

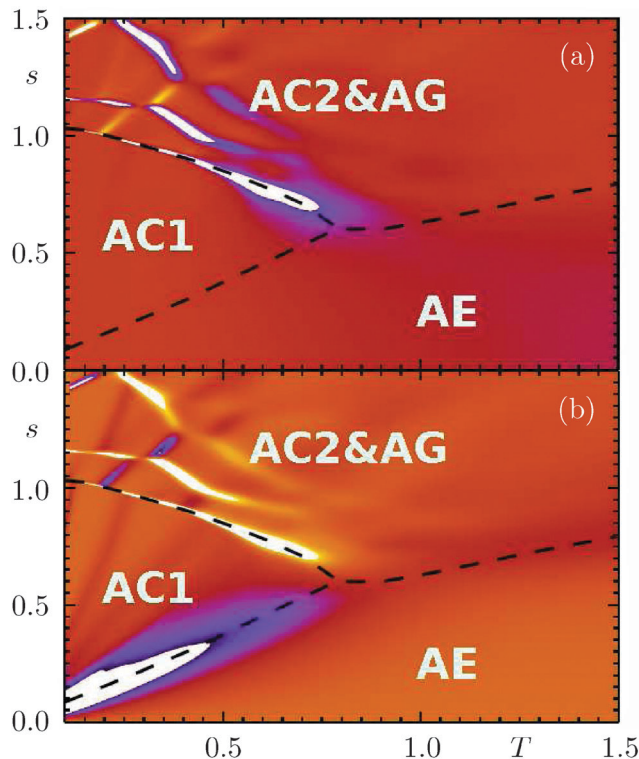


Fig. 8 Density plots of the fluctuations of (a) the number of surface contacts,  $d\langle n_s \rangle / dT$ , and (b) the number of monomer–monomer contacts,  $d\langle n_m \rangle / dT$  as functions of  $s$  and  $T$  for the 503mer. The brighter the shade, the stronger the fluctuation. Dashed black lines separate the structural phases as identified from the analysis of the specific-heat profile shown in Fig. 6.

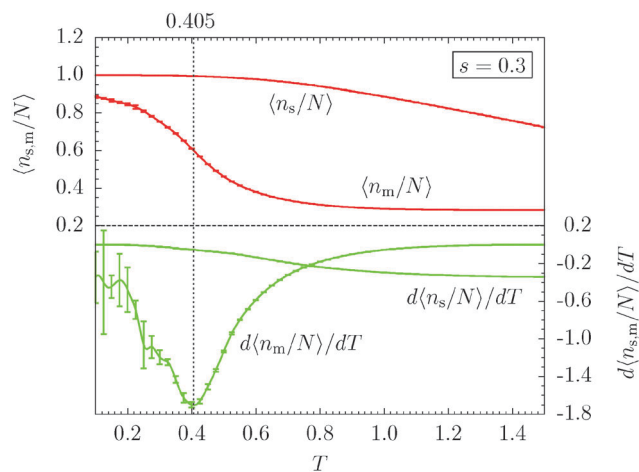


Fig. 9 Suitable order parameters: average numbers of monomer–surface ( $\langle n_s \rangle$ ) and monomer–monomer contacts ( $\langle n_m \rangle$ ) of the polymer with  $N = 503$  beads, and their respective fluctuations  $d\langle n_{s,m} \rangle / dT$  as functions of temperature  $T$  for  $s = 0.3$ . The  $\langle n_m \rangle$  fluctuation near  $T = 0.41$  signals the  $AC1 \rightleftharpoons AE$  transition. The number of surface contacts  $n_s$  remains almost unchanged in this region.

*i.e.*, for  $s > 0$ , the changes of contact numbers are anticorrelated. This dependence of the fluctuations of otherwise independent order parameters upon each other renders the transition that is

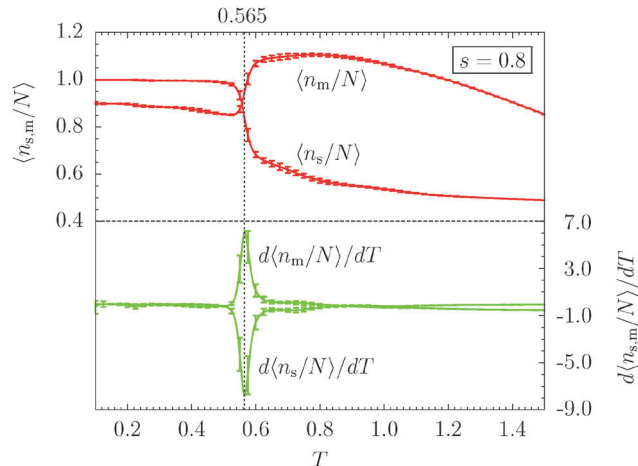


Fig. 10 The same as in Fig. 9 for  $s = 0.8$ . Now both parameters exhibit thermal activity and interlock: the  $AC1 \rightleftharpoons AC2&AG$  transition at  $T \approx 0.57$  is clearly characterized by a correlated increase of monomer–monomer contacts upon a decreasing number of surface contacts.

associated with  $d\Gamma_{E_s} / dT = 0$  a cooperative effect. In this scenario, the order parameters are interlocking, because a change in the fluctuation behavior of one order parameter is inevitably connected to an alteration of the other one in accordance with eqn (15). Most striking is the situation where the relation (15) is satisfied by  $d\Gamma_{n_s} / dT = d\Gamma_{n_m} / dT = 0$ , in which case the fluctuations of energy and both order parameters are extremal at the same temperature. This is not at all typical in transitions of finite systems. This interlocking scenario is particularly apparent for the topological transition from AC1 to AC2&AG. For  $s = 0.8$ , as shown in Fig. 10, both contact numbers are perfectly anticorrelated at the transition point ( $T \approx 0.57$ ).

If only one of the order-parameter fluctuations is extremal, the peak/valley locations of the heat capacity and this order-parameter fluctuation may differ. The other order parameter mixes in and its contributing fluctuation makes the extremal locations of the other quantities vary, to satisfy eqn (14). This is the more common scenario for transitions in finite systems. The transition behavior from AC1 to AE is generally of this kind. For  $s = 0.3$ , as shown in Fig. 9, only the monomer–monomer contact number fluctuates violently at this transition ( $T \approx 0.41$ ), whereas the number of surface contacts remains almost constant. In this case the transition temperature difference of the estimates from  $\Gamma_{E_s}$  and  $\Gamma_{n_m}$  is negligible, because  $\Gamma_{n_s} \approx 0$  and also  $d\Gamma_{n_s} / dT \approx 0$ . However, the difference can be rather large, particularly at entropic transitions that occur at comparatively high temperatures (*cf.*, *e.g.*, the discussion in ref. 20 and 21).

This can be generalized for the corresponding sections of the phase diagram. The density plots of the contact-number fluctuations shown in Fig. 8 for the section of  $(T, s)$  parameter space that contains these phases, exhibit very nicely the differences of transition behavior along the entire  $AC1 \rightleftharpoons AC2&AG$  and  $AC1 \rightleftharpoons AE$  transition lines, respectively. If in both figures, Fig. 8(a) and (b), pronounced bright regions are found in the same sections of the phase diagrams, both order parameters

have interlocked. Beyond the topological transition  $AC1 \Leftrightarrow AC2&AG$ , we find that similar interlocking occurs if the solvent quality is reduced further, which enhances the population of compact three-dimensional, higher-layered adsorbed conformations in  $AC2$ .

## V. Summary

By means of advanced generalized-ensemble contact-density chain-growth methods, we have investigated structural phases of a flexible, self-interacting polymer adsorbed at a homogeneous substrate and studied the transition behavior in much more detail than has been dedicated before. In this study, we focused on the understanding of the thermal activity of two obvious order parameters of the system, the numbers of monomer–monomer and monomer–surface contacts, respectively.

By introducing the free energy as a function of these order parameters, we could locate all free-energy minima in a large parameter space (temperature and solvent quality). Based on the analysis of the structural microphases and their stability, the complex structure of the microphase diagram, which is typically inaccessible, could be revealed and the transition lines located. The structural phases were identified as adsorbed-compact single-layer ( $AC1$ ), higher-order layered compact and globular ( $AC2&AG$ ), as well as adsorbed expanded ( $AE$ ).

In a complementary approach, we constructed the phase diagram based on the free-energy minima in contact-number space, which yielded interesting insights into the nature of transition paths passing these transitions under different solvent conditions. Ultimately, we performed a canonical statistical analysis of the fluctuations of energy and contact numbers in the space of the external parameters temperature and solvent quality. Since the fluctuations of energy and order parameters are not independent of each other, we found that in the extreme case of anticorrelated behavior the order parameters interlock, in which case the transition temperatures estimated from the heat capacity and from the fluctuations of the contact numbers coincide. This scenario applies to the topological transition between  $AC1$  and  $AC2&AG$  (poor solvent), whereas the behavior is different if the polymer goes through the  $AC1 \Leftrightarrow AE$  transition (good solvent).

The occurrence of interlocking can be interpreted as cooperative behavior and as an indicator that the set of corresponding order parameters is sufficient for the understanding of this transition. In future works, the significance of the transitions in the adsorption regime needs to be verified by thorough scaling analyses. It is also appealing to investigate the adsorption behavior for brushes of grafted polymers.

## Acknowledgements

This work has been supported partially by the NSF under Grant No. DMR-1207437 and by CNPq (National Council for Scientific and Technological Development, Brazil) under Grant No. 402091/2012-4.

## References

- 1 M. N. Rosenbluth and A. W. Rosenbluth, *J. Chem. Phys.*, 1955, **23**, 356.
- 2 N. Madras and A. D. Sokal, *J. Stat. Phys.*, 1988, **50**, 109.
- 3 I. Carmesin and K. Kremer, *Macromolecules*, 1988, **21**, 2819.
- 4 H. P. Deutsch and K. Binder, *J. Chem. Phys.*, 1991, **94**, 2294.
- 5 P. Grassberger and R. Hegger, *J. Chem. Phys.*, 1995, **102**, 6881.
- 6 P. Grassberger, *Phys. Rev. E: Stat. Phys., Plasmas, Fluids, Relat. Interdiscip. Top.*, 1997, **56**, 3682.
- 7 F. Rampf, W. Paul and K. Binder, *Europhys. Lett.*, 2005, **70**, 628.
- 8 F. Rampf, W. Paul and K. Binder, *J. Polym. Sci., Part B: Polym. Phys.*, 2006, **44**, 2542.
- 9 T. Vogel, M. Bachmann and W. Janke, *Phys. Rev. E: Stat., Nonlinear, Soft Matter Phys.*, 2007, **76**, 061803.
- 10 M. Bachmann, *Thermodynamics and Statistical Mechanics of Macromolecular Systems*, Cambridge University Press, Cambridge, 2014.
- 11 K. A. Dill, *Biochemistry*, 1985, **24**, 1501.
- 12 K. F. Lau and K. A. Dill, *Macromolecules*, 1989, **22**, 3986.
- 13 K. Yue and K. A. Dill, *Proc. Natl. Acad. Sci. U. S. A.*, 1995, **92**, 146.
- 14 T. C. Beutler and K. A. Dill, *Protein Sci.*, 1996, **5**, 2037.
- 15 H. Frauenkron, U. Bastolla, E. Gerstner, P. Grassberger and W. Nadler, *Phys. Rev. Lett.*, 1998, **80**, 3149.
- 16 Y. Cui, W. H. Wong, E. Bornberg-Bauer and H. S. Chan, *Proc. Natl. Acad. Sci. U. S. A.*, 2002, **99**, 809.
- 17 A. Irbäck and C. Troein, *J. Biol. Phys.*, 2002, **28**, 1.
- 18 H.-P. Hsu, V. Mehra, W. Nadler and P. Grassberger, *J. Chem. Phys.*, 2003, **118**, 444.
- 19 H.-P. Hsu, V. Mehra, W. Nadler and P. Grassberger, *Phys. Rev. E: Stat., Nonlinear, Soft Matter Phys.*, 2003, **68**, 21113.
- 20 M. Bachmann and W. Janke, *Phys. Rev. Lett.*, 2003, **91**, 208105.
- 21 M. Bachmann and W. Janke, *J. Chem. Phys.*, 2004, **120**, 6779.
- 22 R. Schiemann, M. Bachmann and W. Janke, *J. Chem. Phys.*, 2005, **122**, 114705.
- 23 G. Shi, T. Vogel, T. Wüst, Y. W. Li and D. P. Landau, *Phys. Rev. E: Stat., Nonlinear, Soft Matter Phys.*, 2014, **90**, 033307.
- 24 K. Qi and M. Bachmann, *J. Chem. Phys.*, 2014, **141**, 074101.
- 25 M. P. Taylor, W. Paul and K. Binder, *Phys. Rev. E: Stat., Nonlinear, Soft Matter Phys.*, 2009, **79**, 050801(R).
- 26 T. Vrbová and S. G. Whittington, *J. Phys. A: Math. Gen.*, 1996, **29**, 6253.
- 27 T. Vrbová and S. G. Whittington, *J. Phys. A: Math. Gen.*, 1998, **31**, 3989.
- 28 Y. Singh, D. Giri and S. Kumar, *J. Phys. A: Math. Gen.*, 2001, **34**, L67.
- 29 R. Rajesh, D. Dhar, D. Giri, S. Kumar and Y. Singh, *Phys. Rev. E: Stat., Nonlinear, Soft Matter Phys.*, 2002, **65**, 056124.
- 30 M. Bachmann and W. Janke, *Phys. Rev. Lett.*, 2005, **95**, 058102.
- 31 M. Bachmann and W. Janke, *Phys. Rev. E: Stat., Nonlinear, Soft Matter Phys.*, 2006, **73**, 041802.
- 32 J. Krawczyk, T. Prellberg, A. L. Owczarek and A. Rechnitzer, *Europhys. Lett.*, 2005, **70**, 726.

- 33 J. Krawczyk, T. Prellberg, A. L. Owczarek and A. Reznitzer, *J. Stat. Mech.: Theory Exp.*, 2004, P10004.
- 34 M. Bachmann and W. Janke, *Phys. Rev. E: Stat., Nonlinear, Soft Matter Phys.*, 2006, **73**, 020901(R).
- 35 J. Luettmer-Strathmann, F. Rampf, W. Paul and K. Binder, *J. Chem. Phys.*, 2008, **128**, 064903.
- 36 A. D. Swetnam and M. P. Allen, *Phys. Chem. Chem. Phys.*, 2009, **11**, 2046.
- 37 Y. W. Li, T. Wüst and D. P. Landau, *Phys. Rev. E: Stat., Nonlinear, Soft Matter Phys.*, 2013, **87**, 012706.
- 38 M. P. Taylor and J. Luettmer-Strathmann, *J. Chem. Phys.*, 2014, **141**, 204906.
- 39 P. H. L. Martins and M. Bachmann, *Acta Phys. Pol., B*, 2015, **46**, 1219.
- 40 T. Prellberg and J. Krawczyk, *Phys. Rev. Lett.*, 2004, **92**, 120602.
- 41 M. Möddel, M. Bachmann and W. Janke, *J. Phys. Chem. B*, 2009, **113**, 3314.
- 42 M. Möddel, W. Janke and M. Bachmann, *Phys. Chem. Chem. Phys.*, 2010, **12**, 11548.
- 43 M. Möddel, W. Janke and M. Bachmann, *Macromolecules*, 2011, **44**, 9013.
- 44 E. Eisenriegler, K. Kremer and K. Binder, *J. Chem. Phys.*, 1982, **77**, 6296.